Supporting Information

Phosphorescent Platinum(II) Alkynyls End-Capped with Benzothiazole Units

Rebeca Lara, Elena Lalinde* and M. Teresa Moreno*[a]

[a] *Departamento de Química-Centro de Síntesis Química de La Rioja, (CISQ), Universidad de La Rioja, 26006, Logroño, Spain. E-mail: elena.lalinde@unirioja.es; teresa.moreno@unirioja.es*

Contents: **Page**

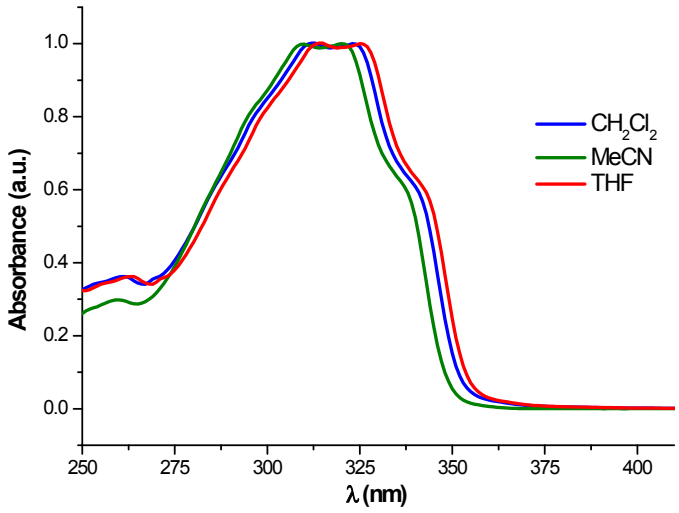

Figure S1. UV-vis absorption spectra of **L**[1] in different solvents (5 x 10^{-5} M) at 298 K.

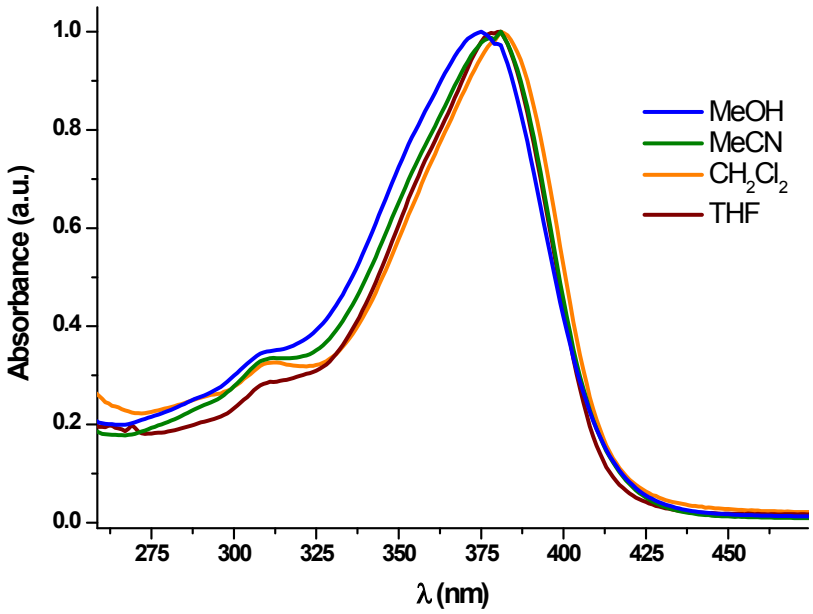

Figure S2. UV-vis absorption spectra of **2** in different solvents (5 x 10^{-6} M) at 298 K.

Table S1. UV-vis absorption maxima of **4** in different solvents, Kamlet-Taft (α, β, π*, δ) empirical solvent polarity parameters and Gutmann's AN and predicted absorption energies.

Solvent	Absorption energy (nm)	Absorption energy (10^3 cm^{-1})	*α*	*β*	*π**	*δ*	*AN*	Predicted K-M absorption energy (10^3 cm^{-1})	Predicted *AN* absorption energy (10^3 cm^{-1})
THF	403	24.82	0	0.55	0.58	0	8	25.10	25.17
Toluene	399	25.08	0	0.11	0.54	1	3.3	25.17	24.87
Acetone	393	25.44	0.08	0.43	0.71	0	12.5	25.51	25.46
DMF	393	25.47	0	0.69	0.88	0	16	25.67	25.68
DMSO	388	25.79	0	0.76	1	0	19.3	25.91	25.89
CH_2Cl_2	383	26.08	0.13	0.1	0.82	0.5	20.4	25.91	25.96
MeCN	379	26.40	0.19	0.4	0.75	0	18.9	25.81	25.86
EtOH	377	26.50	0.86	0.75	0.54	0	37.1	26.71	27.01
MeOH	364	27.57	0.98	0.66	0.6	0	41.3	27.07	27.28
MeOH/H_2O 60:40	362	27.63	1.06	0.58	0.8	0	-	27.62	-
CF_3CH_2OH	356	28.11	1.51	0	0.73	0	53.8	28.40	28.07

Table S2. Emission maxima of **4** in different solvents, Kamlet-Taft (α, β, π*, δ) empirical solvent polarity parameters and Gutmann's AN and predicted absorption energies.

Solvent	Emission energy (nm)	Emission energy (10^3 cm^{-1})	*α*	*β*	*π**	*δ*	*AN*	Predicted K-M emission energy (10^3 cm^{-1})	Predicted *AN* emission energy (10^3 cm^{-1})
THF	550	18.16	0	0.55	0.58	0	8	18.17	18.18
Toluene	552	18.12	0	0.11	0.54	1	3.3	18.09	18.11
Acetone	544	18.37	0.08	0.43	0.71	0	12.5	18.29	18.24
DMF	548	18.25	0	0.69	0.88	0	16	18.28	18.28
DMSO	545	18.35	0	0.76	1	0	19.3	18.32	18.33
DCM	546	18.31	0.13	0.1	0.82	0.5	20.4	18.36	18.34
MeCN	546	18.32	0.19	0.4	0.75	0	18.9	18.36	18.32
EtOH	542	18.44	0.86	0.75	0.54	0	37.1	18.44	18.57
MeOH	541	18.49	0.98	0.66	0.6	0	41.3	18.54	18.63
MeOH/H_2O 60:40	534	18.72	1.06	0.58	0.8	0	-	18.68	-
CF_3CH_2OH	527	18.98	1.51	0	0.73	0	53.8	18.96	18.79

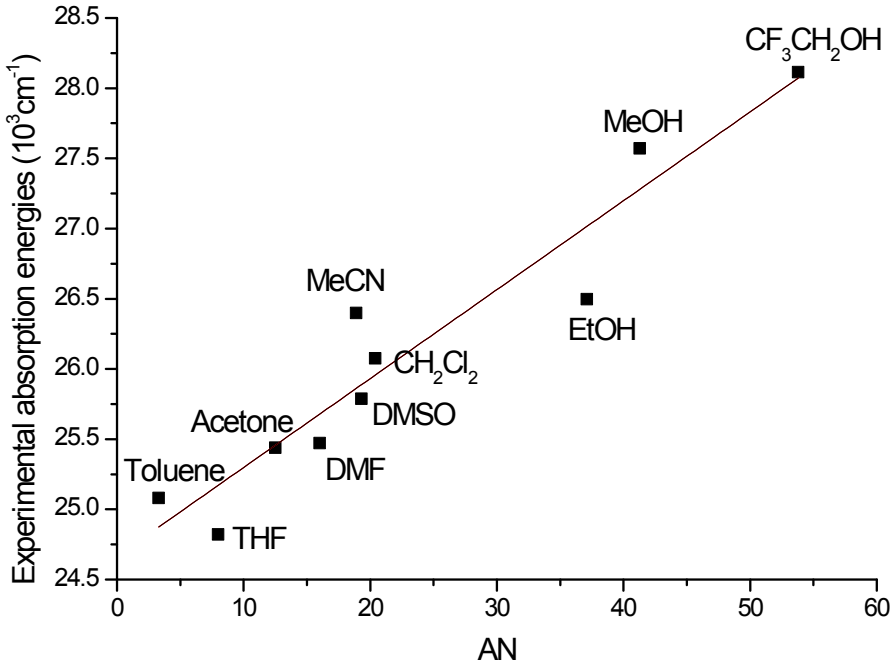

Figure S3. Plot of absorption energy (E_{abs}) of the lowest-energy absorption band of **4** *vs* acceptor numbers of solvents.

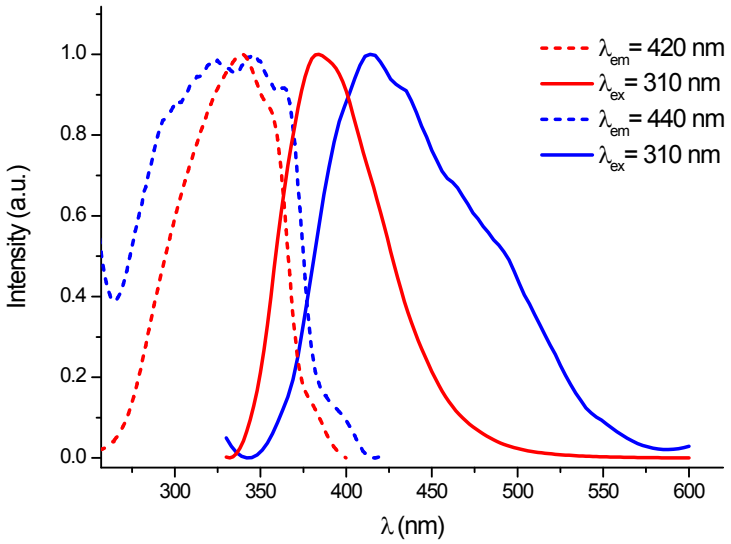

a)

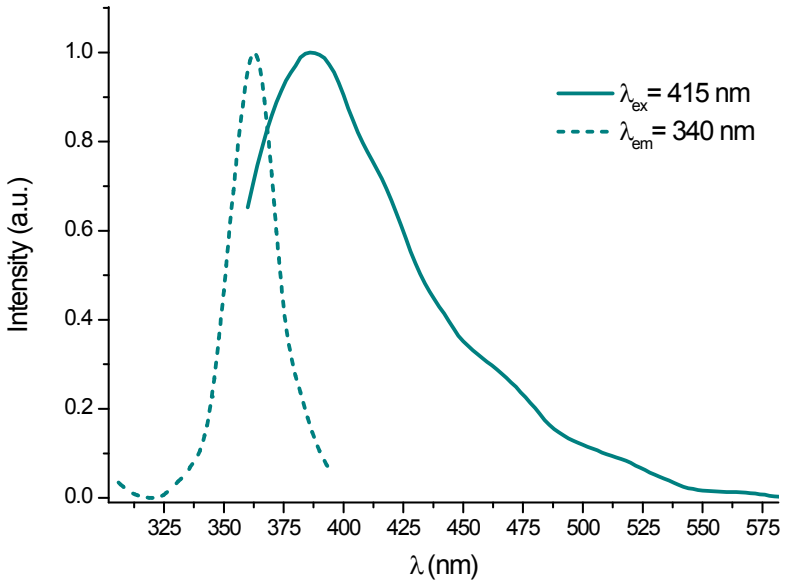

b)

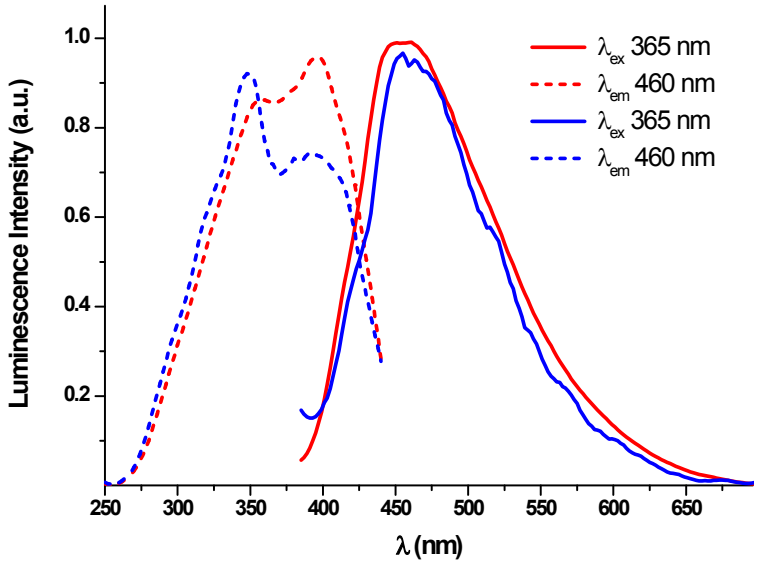

c)

Figure S4. Normalized excitation and emission spectra of **L¹**, a) in CH_2Cl_2 (5 x 10^{-4} M) at 298 K (red) and at 77 K (blue), b) in PMMA (*wt* 1%) at 298 K, c) in the solid state.

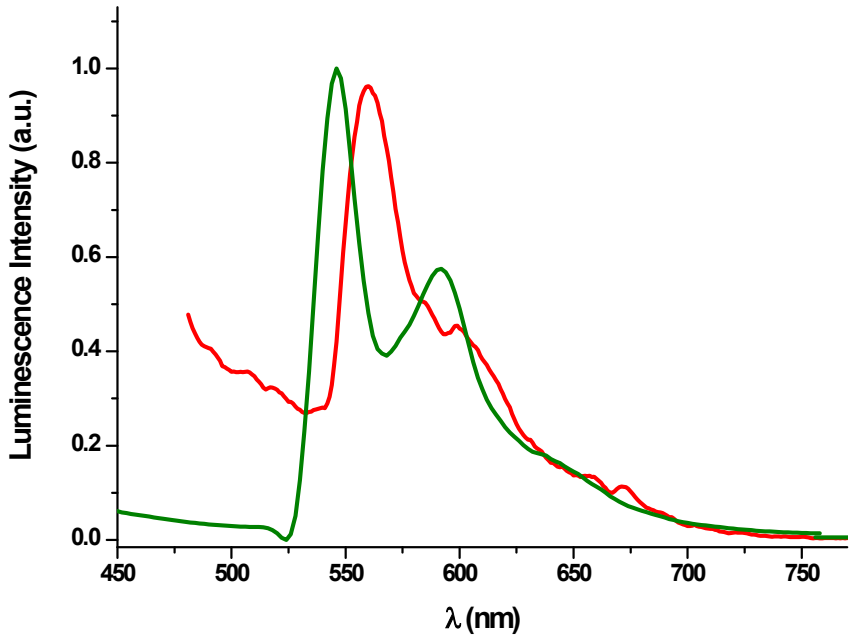

Figure S5. Normalized emission spectra of **4** in solid state (red, λ_{exc} 410 nm) and in CH_2Cl_2 at 77 K (green, λ_{exc} 390 nm)

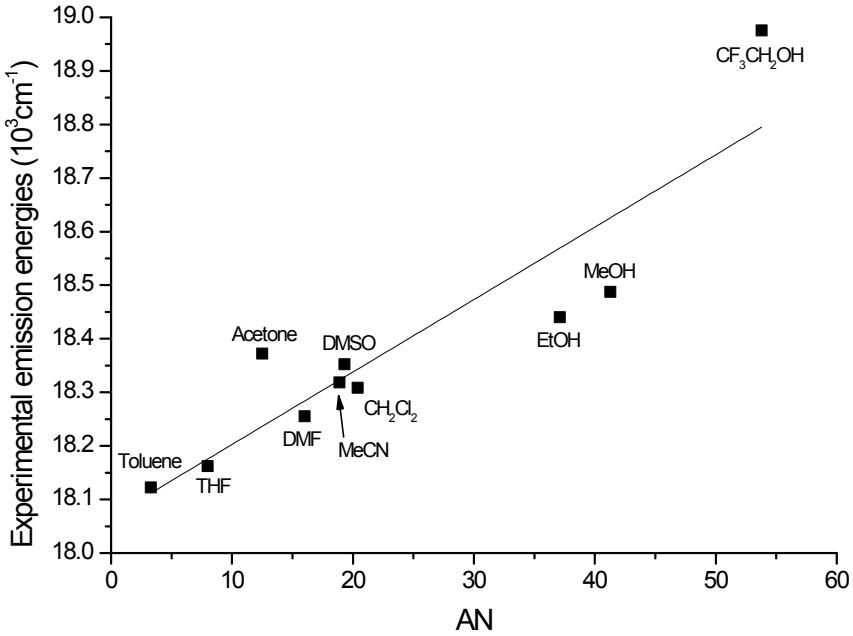

Figure S6. Plot of emission energy ($E_{emission}$) of the lowest-energy absorption band of **4** *vs* acceptor numbers of solvents.

Table S3. DFT optimized geometries for ground state and triplet state of species **2a**, **2b**, **4a**, **4b** and **4a·2H$_2$O** (S_0 in CH_2Cl_2; T_1 in gas phase for **2a**, **2b** and in CH_2Cl_2 for **4a**)

2a (starting from the X-ray structure of molecule A)			
	X-Ray	S_0	T_1
Pt1-C1	2.013(5)	2.019	2.019
Pt1-C16	2.007(5)	2.017	2.016
Pt1-P1	2.2982(13)	2.370	2.363
Pt1-P2	2.3097(14)	2.377	2.367
C1-C2	1.189(7)	1.230	1.248
C16-C17	1.186(7)	1.230	1.229
C1-Pt1-P1	86.82(15)	86.60	86.69
C1-Pt1-P2	91.50(15)	92.47	82.88
Pt1-C1-C2	177.4(4)	177.18	176.13
Pt1-C16-17	176.7(5)	178.39	177.64
Interplanar angle between the Ph rings of both bpt ligands	70.0º	64	63
Angle between the Ph ring of the pbt1 group and the Pt plane	13.5	28	12
Angle between the Ph ring of the pbt2 group and the Pt plane	82.1	89	74
Angle between the Ph and the bt rings of the pbt1 group	12.1	0	0
Angle between the Ph and the bt rings of the pbt2 group	10.3	0	0.5

2b (starting from the X-ray structure of molecule B)			
	X-Ray	S_0	T_1
Pt2-C43	2.008(6)	2.018	1.977
Pt2-P3	2.2919(13)	2.368	2.366
C43-C44	1.181(8)	1.230	1.247
C43-Pt2-P3	88.08(15)	87.17	92.72
Pt2-C43-C44	178.4(5)	179.12	178.85
Interplanar angle between the Ph rings of both bpt ligands	0.0	0	0
Angle between the Ph ring of the pbt groups and the Pt plane	6.1	1	0
Angle between the Ph and the bt rings of the pbt groups	8.8	0.5	0

4a (starting from the X-ray structure)			
	X-Ray	S_0	T_1
Pt-C1	1.987(3)	2.014	2.020
Pt-C2	2.000(3)	2.013	2.020
Pt-C3	2.007(3)	2.020	1.978
Pt-C18	2.005(3)	2.020	1.978
N1-C1	1.153(4)	1.172	1.170
N4-C2	1.148(4)	1.172	1.170
C3-C4	1.203(4)	1.230	1.245
C18-C19	1.208(4)	1.230	1.245
C1-Pt-C2	179.09(10)	179.95	179.94
C1-Pt-C3	88.59(11)	90.10	90.16
C2-Pt-C3	91.11(11)	89.95	89.84
C18-Pt-C3	178.71(11)	179.64	179.31
Pt-C1-N1	177.9(3)	179.95	179.91
Pt-C2-N4	177.2(3)	179.93	179.85
Pt-C3-C4	176.6(3)	179.55	179.13
Pt-C18-C19	177.6(2)	179.48	179.14
Interplanar angle between the Ph rings of both bpt ligands	27.2	13	3
Angle between the Ph ring of the pbt1 group and the Pt plane	44.6	30	4
Angle between the Ph ring of the pbt2 group and the Pt plane	17.4	17	4
Angle between the Ph and the bt rings of the pbt1 group	5.6	2	0
Angle between the Ph and the bt rings of the pbt2 group	10.5	0	0

4b (starting from an orthogonal pbt-pbt model)			
	X-Ray	S_0	
Pt-C1	1.987(3)	2.014	
Pt-C2	2.000(3)	2.014	
Pt-C3	2.007(3)	2.020	
Pt-C18	2.005(3)	2.019	
N1-C1	1.153(4)	1.172	

N4-C2	1.148(4)	1.172	
C3-C4	1.203(4)	1.230	
C18-C19	1.208(4)	1.230	
C1-Pt-C2	179.09(10)	179.95	
C1-Pt-C3	88.59(11)	90.06	
C2-Pt-C3	91.11(11)	90.00	
C18-Pt-C3	178.71(11)	179.93	
Pt-C1-N1	177.9(3)	179.93	
Pt-C2-N4	177.2(3)	179.92	
Pt-C3-C4	176.6(3)	179.91	
Pt-C18-C19	177.6(2)	179.90	
Interplanar angle between the Ph rings of both bpt ligands	27.2	30	
Angle between the Ph ring of the pbt1 group and the Pt plane	44.6	22	
Angle between the Ph ring of the pbt2 group and the Pt plane	17.4	8	
Angle between the Ph and the bt rings of the pbt1 group	5.6	1	
Angle between the Ph and the bt rings of the pbt2 group	10.5	0.7	

4a·2H_2O (starting from the X-ray structure)			
	X-Ray	S_0	T_1
Pt-C1	1.987(3)	2.009	
Pt-C2	2.000(3)	2.009	
Pt-C3	2.007(3)	2.022	
Pt-C18	2.005(3)	2.021	
N1-C1	1.153(4)	1.170	
N4-C2	1.148(4)	1.171	
C3-C4	1.203(4)	1.230	
C18-C19	1.208(4)	1.230	
C1-Pt-C2	179.09(10)	179.9	
C1-Pt-C3	88.59(11)	90.0	
C2-Pt-C3	91.11(11)	90.0	
C18-Pt-C3	178.71(11)	90.0	
Pt-C1-N1	177.9(3)	179.6	
Pt-C2-N4	177.2(3)	179.6	

Pt-C3-C4	176.6(3)	179.9	
Pt-C18-C19	177.6(2)	179.9	
Interplanar angle between the Ph rings of both bpt ligands	27	9	
Angle between the Ph ring of the pbt1 group and the Pt plane	45	46	
Angle between the Ph ring of the pbt2 group and the Pt plane	17	37	
Angle between the Ph and the bt rings of the pbt1 group	6	1	
Angle between the Ph and the bt rings of the pbt2 group	1	2	

2a	
S_0	**T_1**
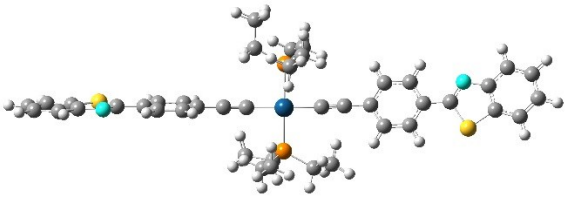	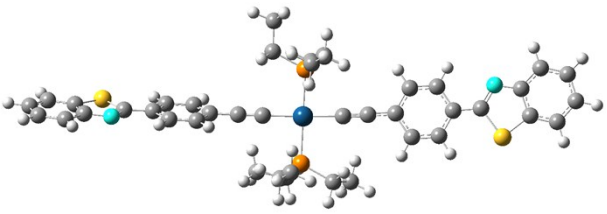

2b	
S_0	**T_1**
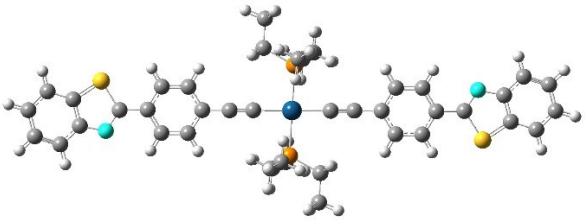	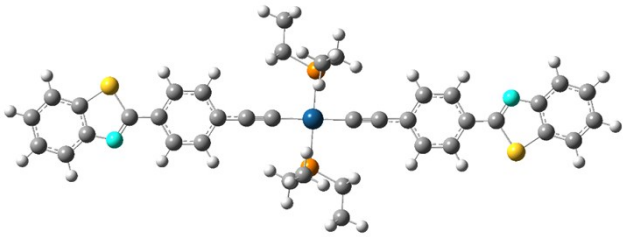

4a	
S_0	**T_1**

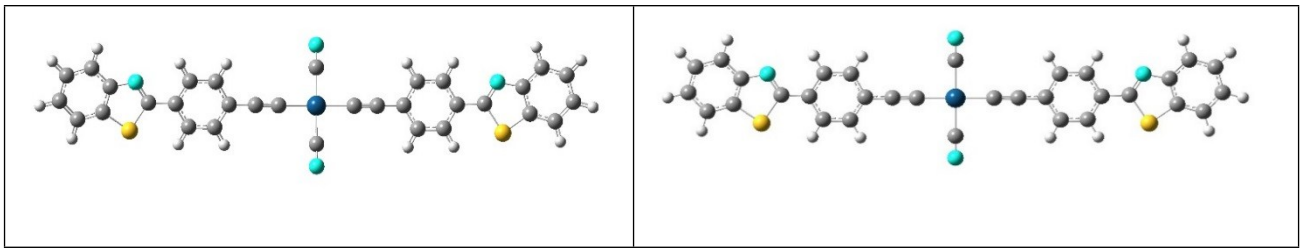

4b	**4a·2H$_2$O**
S$_0$	**S$_0$**
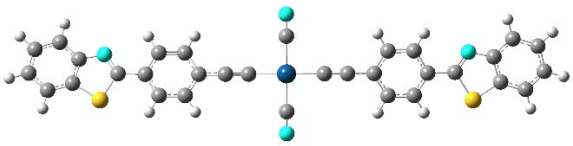	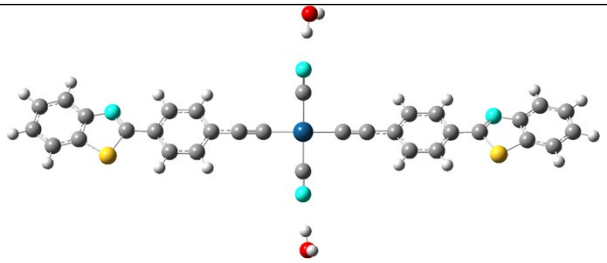

Figure S7. Optimized structures of **2a**, **2b, 4a**, **4b** and **4a·2H$_2$O** in their S_0 states in CH_2Cl_2 and of **2a**, **2b** -gas phase- and **4a** -CH_2Cl_2- in their T_1 states.

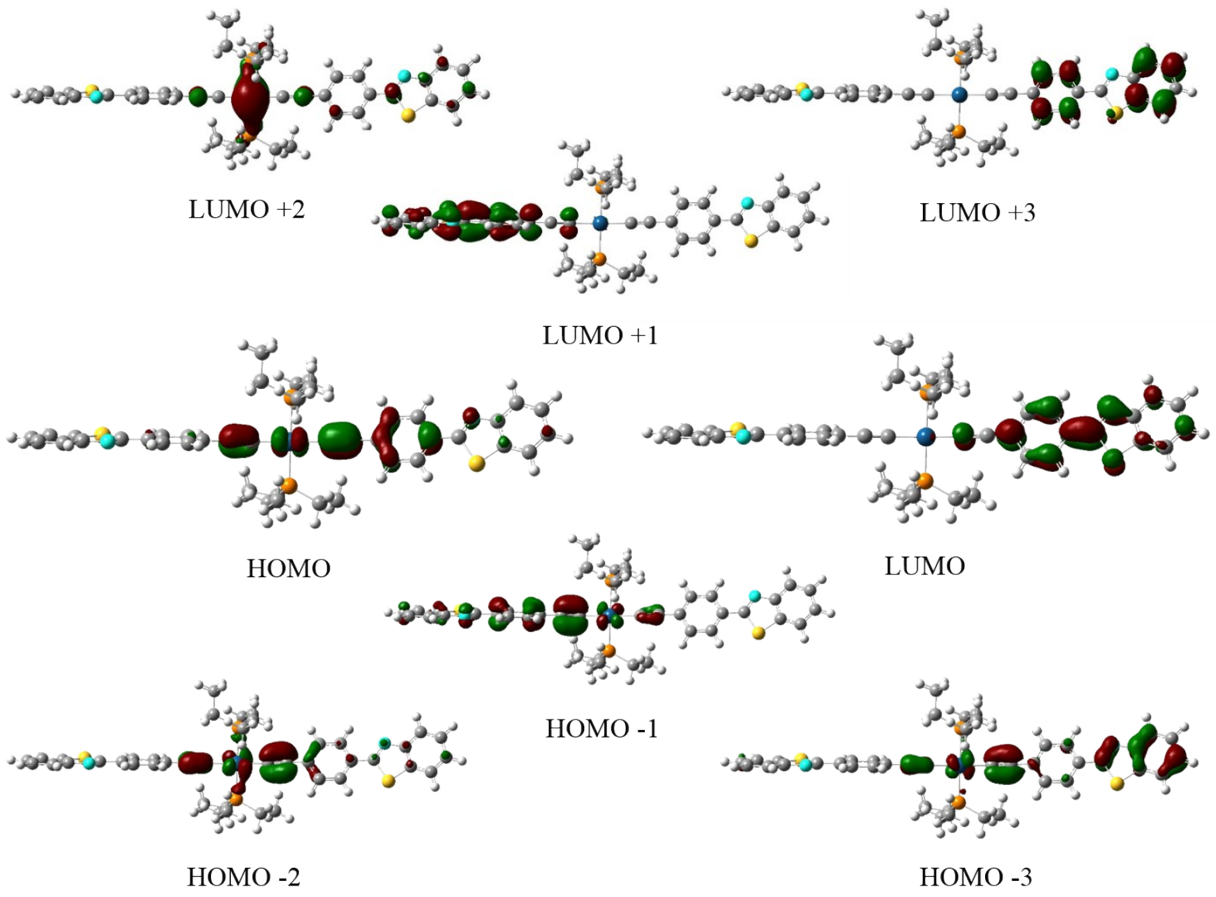

Figure S8. Selected frontier Molecular Orbitals for **2a** in the ground state.

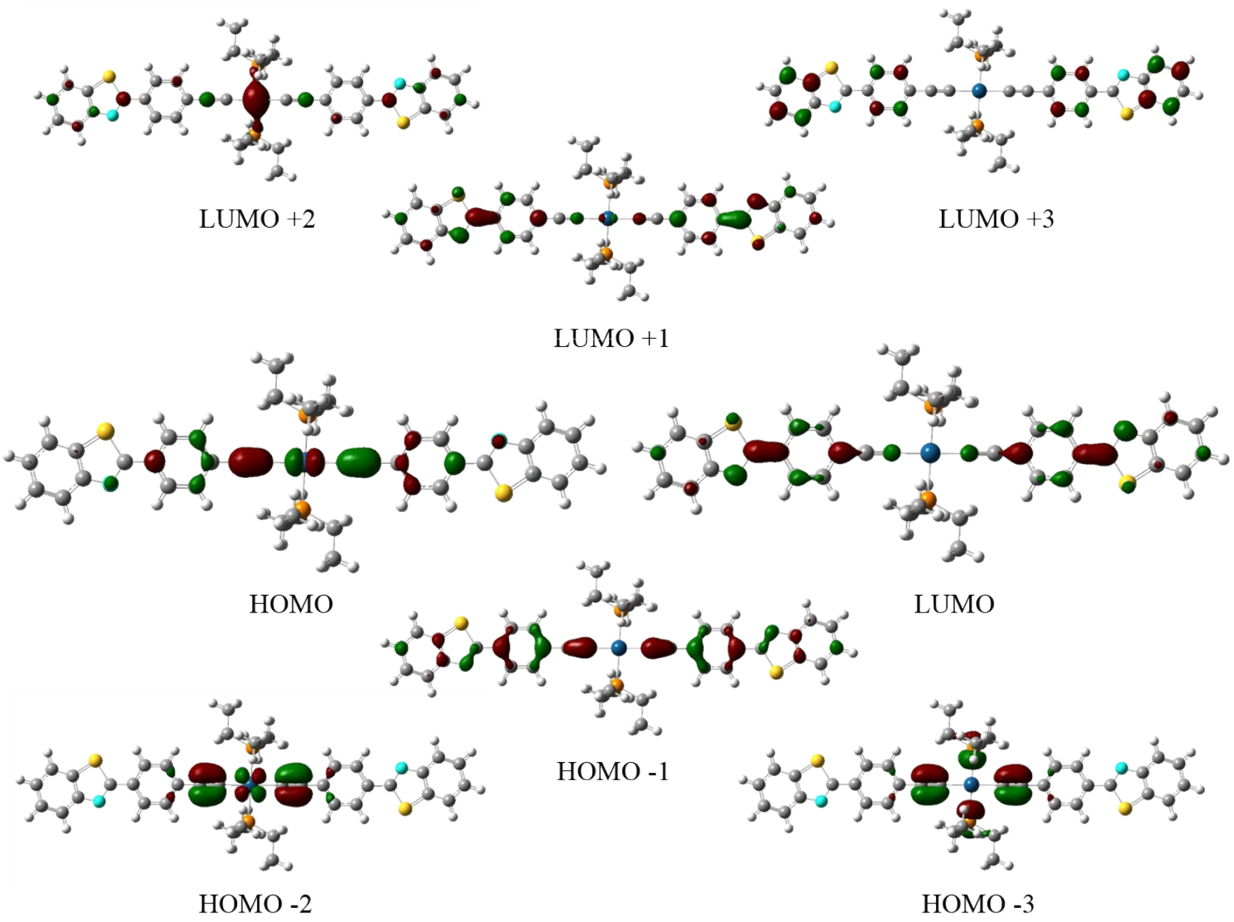

Figure S9. Selected frontier Molecular Orbitals for **2b** in the ground state.

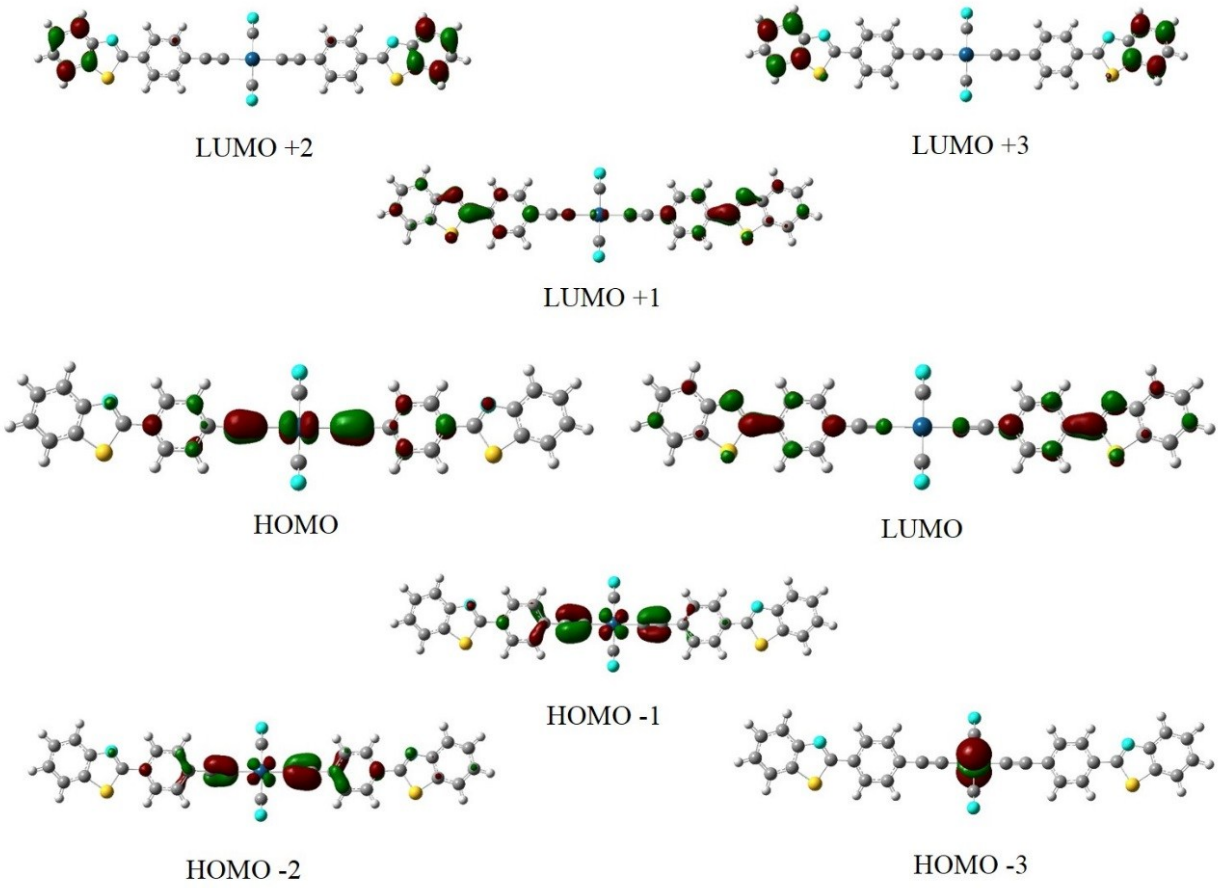

Figure S10. Selected frontier Molecular Orbitals for **4a** in the ground state.

Table S4. Selected vertical excitation energies singlets (S_0) and first triplets computed by TDDFT/SCRF (CH_2Cl_2) with the orbitals involved for **L[1], 2a**, **2b, 4a** and **4a·2H$_2$O**

	State	λ_{ex}(calc)(nm)	f	Transition (% Contribution)
L[1]	S_1	335	1.1186	HOMO→LUMO (97%)
	S_2	312	0.0615	H-1→LUMO (94%)
	S_3	275	0.0131	H-3->LUMO (70%), HOMO->L+1 (24%)
	S_4	267	0.0004	H-5->LUMO (46%), H-4->LUMO (52%)
	S_5	265	0.0367	H-2->LUMO (91%)
	S_6	242	0.0052	H-1->L+3 (13%), HOMO->L+1 (16%), HOMO->L+2 (49%)
	S_7	234	0.0732	H-3->LUMO (20%), HOMO->L+1 (54%), HOMO->L+2 (15%)
	S_8	229	0.0001	HOMO->L+4 (90%)
	S_9	229	0.0512	H-1->L+2 (12%), HOMO->L+3 (67%)
	S_{10}	223	0.087	H-1->L+1 (87%)
	S_{11}	219	0.0001	H-1->L+4 (91%)
2a	T_1	539	-	HOMO→LUMO (72%)
	T_2	528	-	H-1→L+1 (66%), HOMO→L+1 (14%)
	T_3	392	-	H-3→LUMO (11%), HOMO→L+1 (41%)
	S_1	401	2.5214	HOMO→LUMO (85%)
	S_2	386	0.0781	H-1→L+1 (12%), HOMO→L+1 (80%)
	S_3	379	0.0001	H-1→LUMO (85%)
	S_4	370	0.4872	H-1→L+1 (74%), HOMO→L+1 (12%)
	S_5	342	0.0663	H-2→LUMO (78%)
	S_6	322	0.0218	H-2→L+1 (85%)
	S_7	304	0.0287	H-5→LUMO (78%)
	S_8	302	0.1025	H-3→LUMO (29%), HOMO→L+2 (58%)
	S_9	301	0.0746	H-4→L+1 (76%)
	S_{10}	300	0.0216	H-3→LUMO (38%), H-1→L+2 (13%), HOMO→L+2 (23%)
	S_{11}	297	0.0106	H-6→LUMO (91%)
	S_{12}	294	0.0042	H-3→L+1 (11%), H-1→L+2 (63%)
	S_{13}	291	0.0153	H-6→L+1 (54%), H-3→L+1 (28%)
	S_{14}	289	0.0033	H-6→L+1 (42%), H-3→L+1 (37%)
	S_{15}	284	0.0344	H-10→LUMO (38%), HOMO→L+3 (24%), HOMO→L+6 (24%)
2b	T_1	562	-	H-1→L+1 (18%), HOMO→LUMO (74%)
	T_2	529	-	H-1→LUMO (38%), HOMO→L+1 (51%)
	T_3	404	-	H-4→LUMO (24%), H-1→L+1 (24%), HOMO→LUMO (10%), HOMO→L+2 (10%)
	S_1	439	2.4521	HOMO→LUMO (97%)
	S_2	385	0.0000	HOMO→L+1 (99%)
	S_3	367	0.0000	H-2→LUMO (91%)
	S_4	350	0.0000	H-1→LUMO (98%)
	S_5	344	0.0000	H-3→LUMO (39%), H-2→L+1 (57%)
	S_6	327	0.7427	H-1→L+1 (94%)
	S_7	313	0.0000	H-3→LUMO (57%), H-2→L+1 (41%)
	S_8	306	0.0141	H-7→LUMO (97%)
	S_9	305	0.0515	H-6→LUMO (29%), H-5→L+1 (23%), H-4→LUMO (36%)
	S_{10}	305	0.0000	H-6→L+1 (11%), H-5→LUMO (68%), H-4→L+1 (13%)
	S_{11}	302	0.0023	HOMO→L+2 (86%)

	S_{12}	297	0.0017	H-3→L+1 (93%)
	S_{13}	296	0.1772	H-6→LUMO (44%), H-4→LUMO (45%)
	S_{14}	287	0.0000	H-7→L+1 (84%), HOMO→L+7 (13%)
	S_{15}	287	0.0000	H-10→LUMO (24%), H-9→L+1 (11%), HOMO→L+4 (26%), HOMO→L+5 (25%)
4a	T_1	586	-	HOMO→LUMO (74%)
	T_2	555	-	H-2→LUMO (18%), H-1→LUMO (15%), HOMO→L+1 (56%)
	T_3	421	-	H-1→LUMO (48%), H-1→L+1 (10%)
	S_1	463	2.262	HOMO→LUMO (97%)
	S_2	414	0.0156	HOMO→L+1 (91%)
	S_3	402	0.0517	H-2→LUMO (22%), H-1→LUMO (66%)
	S_4	379	0.0592	H-5→LUMO (10%), H-2→L+1 (16%), H-1→L+1 (64%)
	S_5	361	0.0200	H-2→LUMO (69%), H-1→LUMO (23%)
	S_6	344	0.6503	H-2→L+1 (71%), H-1→L+1 (21%)
	S_7	331	0.0089	H-3→LUMO (98%)
	S_8	326	0.0096	H-4→LUMO (98%)
	S_9	323	0.0287	H-5→LUMO (82%)
	S_{10}	316	0.0000	H-3→L+1 (98%)
	S_{11}	309	0.0004	H-4→L+1 (98%)
	S_{12}	307	0.0478	H-5→L+1 (84%)
	S_{13}	300	0.0076	H-8→LUMO (18%), H-7→LUMO (16%), H-7→L+1 (10%), HOMO→L+2 (10%), HOMO→L+3 (12%)
	S_{14}	300	0.037	H-7→LUMO (12%), HOMO→L+3 (12%), HOMO→L+4 (35%)
	S_{15}	300	0.0635	HOMO→L+2 (35%), HOMO→L+4 (19%)
4a·2 H_2O	T_1	567	-	H-2→L+1 (11%), H-1→L+1 (10%), HOMO→LUMO (68%)
	T_2	547	-	H-2→LUMO (17%), H-1→LUMO (19%), HOMO→L+1 (51%)
	T_3	417	-	H-2→LUMO (19%), H-1→LUMO (35%), H-1→L+1 (10%), HOMO→LUMO (13%)
	S_1	445	2.1242	HOMO→LUMO (96%)
	S_2	405	0.0189	HOMO→L+1 (91%)
	S_3	393	0.1759	H-2→LUMO (35%), H-1→LUMO (56%)
	S_4	373	0.0302	H-2→L+1 (26%), H-1→L+1 (53%)
	S_5	359	0.0179	H-2→LUMO (55%), H-1→LUMO (34%)
	S_6	347	0.7147	H-2→L+1 (64%), H-1→L+1 (31%)
	S_7	319	0.0071	H-3→LUMO (98%)
	S_8	308	0.0130	H-5→LUMO (83%)
	S_9	307	0.0000	H-3→L+1 (99%)
	S_{10}	303	0.0099	H-4→LUMO (98%)
	S_{11}	299	0.0877	H-5→L+1 (16%), HOMO→L+2 (31%), HOMO→L+4 (38%)
	S_{12}	298	0.0153	H-8→LUMO (18%), H-7→LUMO (25%), H-7→L+1 (21%), HOMO→L+2 (11%)
	S_{13}	298	0.0189	H-8→LUMO (26%), H-8→L+1 (22%), H-7→LUMO (18%), HOMO→L+3 (11%)
	S_{14}	294	0.0133	H-5→L+1 (67%), HOMO→L+4 (13%)
	S_{15}	291	0.0000	H-4→L+1 (98%)

Table S5. Composition (%) of Frontier MOs in terms of ligands and metals in the ground state for **L[1]**, **2a**, **2b**, **4a** and **4a·2H$_2$O** in CH_2Cl_2.

L[1]

MO	eV	C≡C	Ph	bt
LUMO+5	0.87	12	12	76
LUMO+4	0.23	0	4	95
LUMO+3	-0.19	8	28	64
LUMO+2	-0.30	6	14	80
LUMO+1	-0.45	0	86	14
LUMO	-2.01	10	43	47
HOMO	-6.09	15	35	50
HOMO-1	-6.53	0	1	99
HOMO-2	-7.14	31	22	47
HOMO-3	-7.30	0	99	1
HOMO-4	-7.67	67	8	25
HOMO-5	-7.76	26	4	71

2a

MO	eV	PEt$_3$(1)	PEt$_3$(2)	C≡C(1)	pbt(1)	C≡C(2)	pbt(2)	Pt
LUMO+5	-0.15	0	0	0	5	1	92	0
LUMO+4	-0.26	0	0	0	0	0	100	0
LUMO+3	-0.27	0	0	0	100	0	0	0
LUMO+2	-0.60	12	12	7	21	7	1	40
LUMO+1	-1.74	0	0	1	5	7	86	1
LUMO	-1.81	1	1	7	81	1	5	3
HOMO	-5.34	0	1	27	34	14	7	17
HOMO-1	-5.45	2	2	6	4	33	44	9
HOMO-2	-6.01	4	5	34	19	18	4	16
HOMO-3	-6.39	2	3	23	42	11	8	10
HOMO-4	-6.44	0	0	0	3	0	96	0
HOMO-5	-6.45	0	0	1	94	1	2	2

2b

MO	eV	PEt$_3$(1)	PEt$_3$(2)	C≡C(1)	pbt(1)	C≡C(2)	pbt(2)	Pt
LUMO+5	-0.15	0	0	0	50	0	50	0
LUMO+4	-0.27	0	0	0	50	0	50	0
LUMO+3	-0.27	0	0	0	50	0	50	0
LUMO+2	-0.59	9	9	5	20	5	20	30
LUMO+1	-1.69	0	0	3	46	3	46	1
LUMO	-1.93	1	1	5	41	5	41	5
HOMO	-5.19	0	0	20	21	20	21	18
HOMO-1	-5.78	0	0	13	36	13	36	2
HOMO-2	-5.98	2	2	35	2	35	2	21
HOMO-3	-6.33	18	18	29	2	29	2	3
HOMO-4	-6.43	0	0	2	46	2	46	4
HOMO-5	-6.45	0	0	0	50	0	50	0

4a

MO	eV	CN(1)	CN(2)	C≡C(1)	pbt(1)	C≡C(2)	pbt(2)	Pt
LUMO+5	0.32	0	0	1	57	1	41	0

LUMO+4	0.09	3	3	4	32	4	38	17
LUMO+3	0.05	0	0	0	54	0	46	0
LUMO+2	0.04	1	1	2	41	2	48	6
LUMO+1	-1.27	0	0	4	48	3	44	2
LUMO	-1.45	0	0	4	42	4	45	3
HOMO	-4.53	0	0	21	18	22	19	21
HOMO-1	-5.09	1	1	35	18	21	7	17
HOMO-2	-5.22	1	1	17	16	32	24	10
HOMO-3	-5.67	1	1	1	0	1	0	97
HOMO-4	-5.71	21	20	0	0	0	0	59
HOMO-5	-5.79	5	5	38	2	39	8	2

4a·2H$_2$O

	eV	CN(1)	H_2O(1)	CN(2)	H_2O(2)	C≡C(1)	bt(1)	C≡C(2)	bt(2)	Pt
LUMO+5	0.29	0	0	0	0	1	67	0	32	0
LUMO+4	0.07	3	0	3	0	3	29	3	44	15
LUMO+3	0.04	0	0	0	0	0	54	0	46	0
LUMO+2	0.02	2	0	2	0	3	39	3	37	13
LUMO+1	-1.30	0	0	0	0	3	47	3	45	1
LUMO	-1.45	0	0	0	0	4	44	4	45	2
HOMO	-4.65	0	0	0	0	21	18	22	20	19
HOMO-1	-5.14	1	0	1	0	35	24	17	8	14
HOMO-2	-5.21	1	0	1	0	16	10	35	24	12
HOMO-3	-5.80	0	0	0	0	1	0	1	0	98
HOMO-4	-5.99	19	0	18	0	0	0	0	0	61
HOMO-5	-5.99	3	0	4	0	35	2	39	15	3

Table S6. Composition (%) of Frontier MOs in terms of ligands and metals in the first triplet state for **2a, 2b** (gas phase) and **4a** (in CH_2Cl_2).

2a

	eV	PEt_3(1)	PEt_3(2)	C≡C(1)	pbt(1)	C≡C(2)	pbt(2)	Pt
SOMO	-3.06	0	0	10	84	1	0	4
SOMO-1	-3.75	0	0	19	73	2	0	5

2b

	eV	PEt_3(1)	PEt_3(2)	C≡C(1)	pbt(1)	C≡C(2)	pbt(2)	Pt
SOMO	-2.63	2	2	8	36	8	36	9
SOMO-1	-4.17	0	2	18	26	18	26	13

4a

	eV	CN(1)	CN(2)	C≡C(1)	pbt(1)	C≡C(2)	pbt(2)	Pt
SOMO	-2.28	1	1	6	41	6	41	5
SOMO-1	-3.73	0	0	20	22	20	22	17

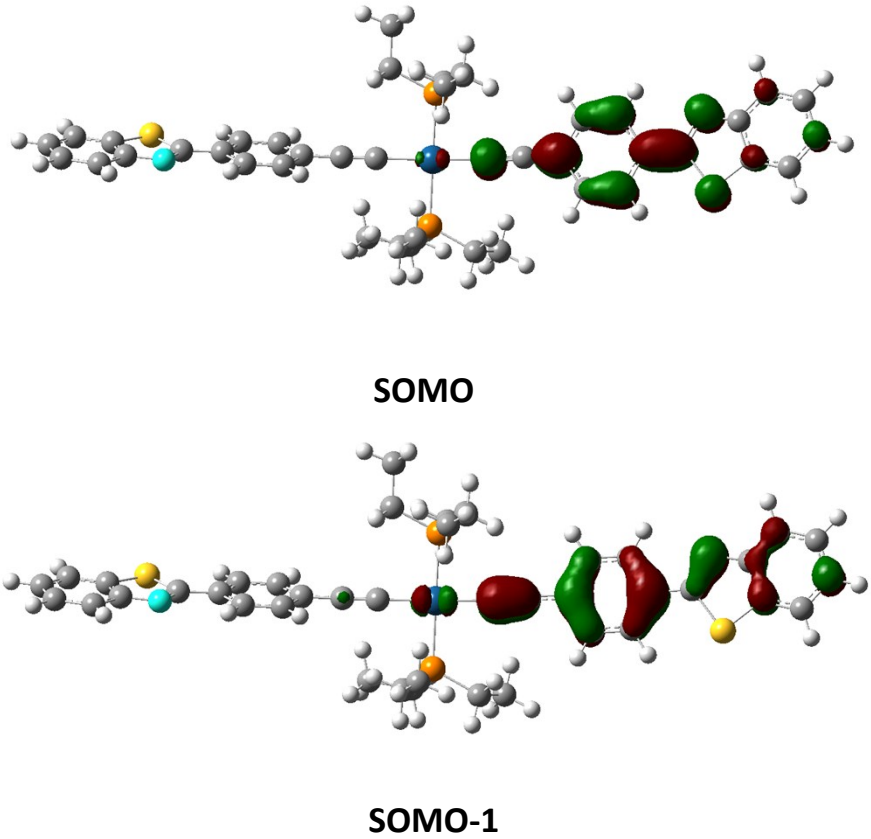

Figure S11. Frontier orbitals plots obtained by DFT for the first triplet state of **2a**.

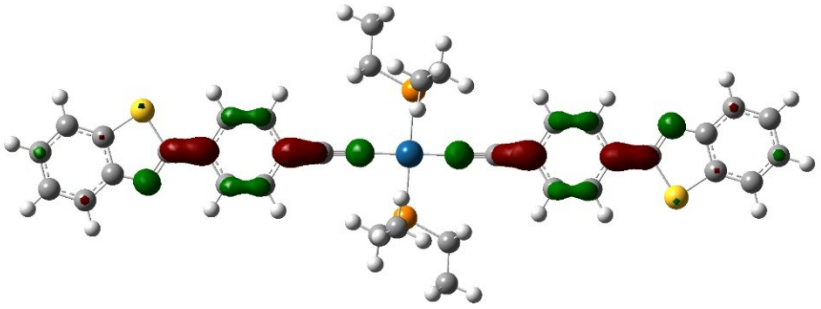

SOMO

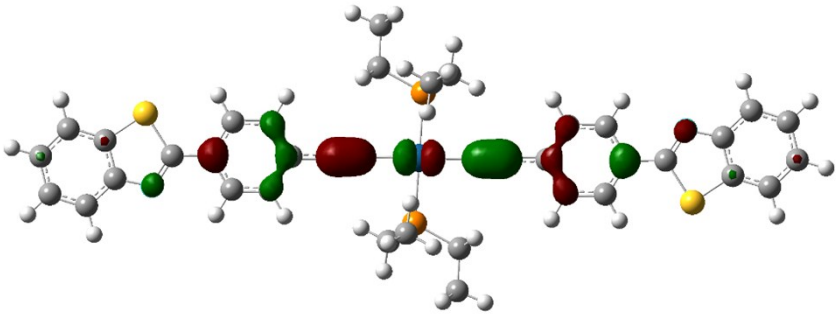

SOMO-1

Figure S12. Frontier orbitals plots obtained by DFT for the first triplet state of **2b**.

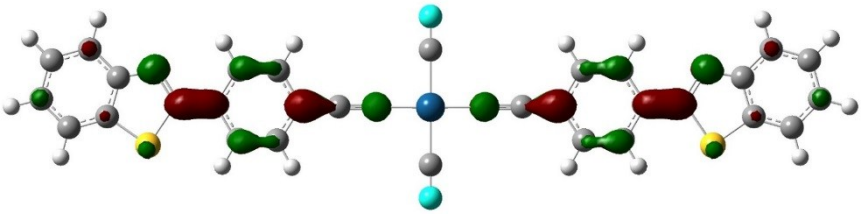

SOMO

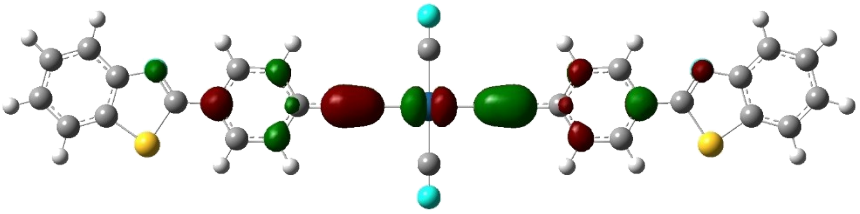

SOMO-1

Figure S13. Frontier orbitals plots obtained by DFT for the first triplet state of **4a**.

Complete reference

(40) Gaussian 09, Revision B.01, M. J. Frisch, G. W. Trucks, H. B. Schlegel, G. E. Scuseria, M. A. Robb, J. R. Cheeseman, G. Scalmani, V. Barone, B. Mennucci, G. A. Petersson, H. Nakatsuji, M. Caricato, X. Li, H. P. Hratchian, A. F. Izmaylov, J. Bloino, G. Zheng, J. L. Sonnenberg, M. Hada, M. Ehara, K. Toyota, R. Fukuda, J. Hasegawa, M. Ishida, T. Nakajima, Y. Honda, O. Kitao, H. Nakai, T. Vreven, J. J. A. Montgomery, J. E. Peralta, F. Ogliaro, M. Bearpark, J. J. Heyd, E. Brothers, K. N. Kudin, V. N. Staroverov, T. Keith, R. Kobayashi, J. Normand, K. Raghavachari, J. C. A. Rendell, Burant, S. S. Iyengar, J. Tomasi, M. Cossi, N. Rega, J. M. Millam, M. Klene, J. E. Knox, J. B. Cross, V. Bakken, C. Adamo, J. Jaramillo, R. Gomperts, R. E. Stratmann, O. Yazyev, A. J. Austin, R. Cammi, C. Pomelli, J. W. Ochterski, R. L. Martin, K. Morokuma, V. G. Zakrzewski, G. A. Voth, P. Salvador, J. J. Dannenberg, S. Dapprich, A. D. Daniels, O. Farkas, J. B. Foresman, J. V. Ortiz, J. Cioslowski and D. J. Fox, Gaussian, Inc., Wallingford CT, 2010.